applied optics

Large-mode-area soliton fiber oscillator mode-locked using NPE in an all-PM self-stabilized interferometer

Marvin Edelmann,[1,2,*] Malek M. Sedigheh,[1,2] Yi Hua,[3] Erwin C. Vargas,[1,2] Mikhail Pergament,[1] and Franz X. Kärtner[1,2]

[1]Center for Free-Electron Laser Science CFEL, Deutsches Elektronen-Synchrotron DESY, Notkestr. 85, 22607 Hamburg, Germany
[2]Department of Physics, Universität Hamburg, Jungiusstr. 9, 20355 Hamburg, Germany
[3]Deutsches Elektronen-Synchrotron DESY, Notkestr. 85, 22607 Hamburg, Germany
*marvin.edelmann@desy.de

Received 13 December 2022; revised 24 January 2023; accepted 26 January 2023; posted 27 January 2023; published 21 February 2023

In this work, we investigate an approach to scale up the output pulse energy in an all-polarization-maintaining 17.3 MHz Yb-doped fiber oscillator via implementation of a 25 μm core-diameter large-mode-area fiber. The artificial saturable absorber is based on a Kerr-type linear self-stabilized fiber interferometer, enabling non-linear polarization rotation in polarization-maintaining fibers. Highly stable mode-locked steady states in the soliton-like operation regime are demonstrated with 170 mW average output power and a total output pulse energy of ∼10 nJ distributed between two output ports. An experimental parameter comparison with a reference oscillator constructed with 5.5 μm core-sized standard fiber components reveals an increase of pulse energy by a factor of 36 with simultaneously reduced intensity noise in the high-frequency range > 100 kHz.

https://doi.org/10.1364/AO.482184

1. INTRODUCTION

Mode-locked fiber oscillators for the generation of stable femtosecond pulse trains are key elements for many state-of-the-art scientific and industrial applications including synchronization and timing [1], biological imaging and spectroscopy [2], seeding of high-power lasers [3], and photonic microwave generation [4]. The output characteristics of the oscillator in conjunction with its parameter stability and resistance against environmental perturbations determine the overall system performance and robustness in industrial applications. In particular, the characteristics of the saturable absorber (SA) for initiation and stabilization of the mode-locked steady states play a crucial role as they often limit the achievable parameters with respect to optical bandwidth, intracavity power, and output pulse energy [5,6]. For more than three decades, artificial SA mechanisms based on the optical Kerr effect have revealed themselves as promising candidates for next-generation fiber oscillator technology. Fiber oscillators mode-locked with non-linear amplifying/optical loop mirrors (NALM/NOLM) [7–9] or linear self-stabilized fiber interferometers (LSIs) based on non-linear polarization evolution (NPE) [10] with all-polarization-maintaining (PM) structures routinely achieve state-of-the-art environmental stability [11], low timing jitter and intensity noise [12]. In contrast to real SAs such as semiconductor saturable absorber mirrors, SAs based on the non-resonant optical Kerr effect allow for large optical bandwidths and short pulse durations while being robust against optical damage and parameter degradation [13]. Besides these advantages, there are limitations associated with the large round-trip non-linear phase shift due to the strong confinement of the laser mode over the full length of fiber segments. These non-linear phase shifts limit the obtainable intracavity pulse energy as multi-pulse formation or breakthrough of continuous-wave lasing occurs above a certain threshold, which ultimately deteriorates the stability of the mode-locked state [14,15]. The limited output pulse energy often necessitates an increased system complexity, e.g., in the form of additional amplification stages. It is further associated with deteriorated oscillator noise parameters in terms of intensity and phase fluctuations [16,17]. Different approaches to overcome this limitation have been the subject of intensive research over the last decade. Besides techniques based on precise dispersion management to reduce the average peak power of the intracavity pulse in the dissipative soliton [18] or stretched-pulse regime [19], other works further investigate the possibility of periodic intracavity coherent pulse division and recombination [20,21] as well as periodic spectral re-shaping in Mamyshev oscillators [22]. In NALM/NOLM mode-locked lasers, the scaling of

the core size with large-mode-area (LMA) fibers has further enabled a significant increase of obtainable pulse energy due to the quadratic dependence on the core diameter [23,24].

In this work, we demonstrate for the first time a Kerr-type LSI mode-locked fiber oscillator using 25 μm core diameter LMA fibers. The 17.3 MHz Yb-doped all-PM oscillator allows stable mode-locking in the soliton-like regime with a total pulse energy of 10 nJ and average power of 170 mW, distributed between two output ports. An experimental comparison with a reference oscillator operating at identical repetition rate and net dispersion shows that the core-diameter enlargement from 5.5 μm to 25 μm results in an increase of the output pulse energy by a factor of 36. Further, the LSI-LMA oscillator shows an intensity noise reduction of ∼ 8 dB in the high-frequency range >20 kHz compared to the reference oscillator.

2. EXPERIMENTAL SETUP AND MEASUREMENTS

A. LSI-LMA Oscillator Setup and Mode-Locking Mechanism

The experimental setup of the LSI mode-locked LMA oscillator is shown in Fig. 1(a). The active fiber cavity includes a pump-beam combiner to couple the pump light generated by an 18 W wavelength-stabilized multimode laser diode at 976 nm into the cladding of a 2 m Yb-doped PM large-mode-area (Yb-PLMA) fiber. The Yb-PLMA fiber (Liekki Yb1200 25/250DC-PM) has a core diameter of 25 μm, a numerical aperture of 0.065, and a peak cladding absorption of 10.6 dB/m at 976 nm. Based on numerical results obtained with the commercial software "RP Photonics," the Yb-PLMA fiber is coiled on a 30 mm radius aluminum coil which corresponds to a theoretical propagation loss of ∼2 dB and ∼20 dB for the LP01 and LP11 modes, respectively. As an additional filter for remaining power in high-order transverse modes, the PLMA segment is spliced to mode-field adapters (MFA1/2) at both ends, tapering the LMA fiber to 0.25 m short pieces of 5.5 μm core-diameter PM fiber (PM-SMF1/2, Coherent PM980-XP). Two fiber collimators (C1/2) couple the light into free-space arms. On the side of C2, a Faraday mirror arrangement consisting of a Faraday rotator (FR) and the end mirror M2 ensure the backreflection and 90° polarization rotation of the intracavity field. The free-space arm on the side of C1 contains a transmission grating pair (1000 lines/mm) for dispersion management, a polarization beam splitter (PBS), and the non-reciprocal phase bias consisting of a FR, a quarter-wave plate (QWP), and a half-wave plate (HWP). To maintain a consistent frame of reference, the fast axis of the PM fiber segment is aligned to the transmission axis of the PBS (subsequently referred to as x axis), and all rotation angles are measured according to the mathematical standard definition. The repetition rate of the laser is 17.3 MHz with a fixed net dispersion of ~ -0.121 ps^2, ensuring a mode-locked operation in the soliton-like regime.

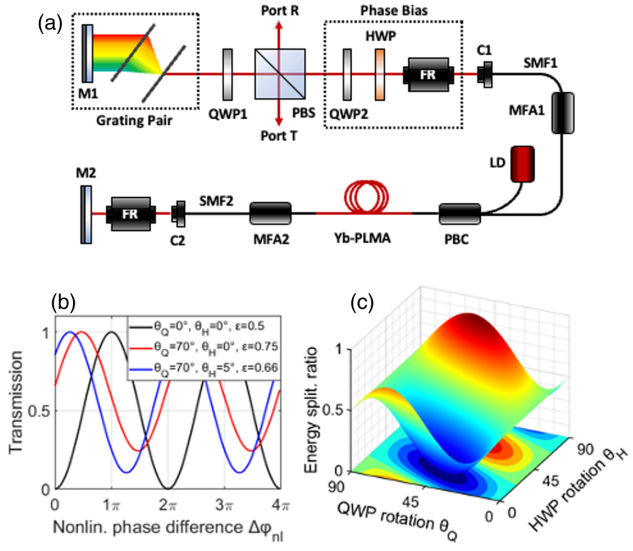

Fig. 1. (a) Experimental setup of the LSI mode-locked LMA oscillator. M, mirror; GP, grating pair; QWP, quarter-wave plate; PBS, polarization beam splitter; HWP, half-wave plate; FR, Faraday rotator; C, collimator; PM-SMF, polarization-maintaining single-mode fiber; MFA, mode-field adapter; LD, laser diode; PBC, pump-beam combiner; Yb-PLMA, ytterbium-doped polarization-maintaining large-mode-area fiber. (b) Transmission $T(\Delta\varphi_{nl})$ as function of the non-linear phase difference $\Delta\varphi_{nl}$ for characteristic values of the QWP rotation angle θ_Q and the HWP rotation angle θ_H in the non-reciprocal phase bias. (c) Energy splitting-ratio ε between the polarization modes in the PM-fiber LSI as function of θ_Q and θ_H.

The mode-locking mechanism of the LSI-LMA oscillator is based on the accumulation of a differential non-linear phase shift $\Delta\varphi_{nl}$ between the orthogonal polarization modes in the PM-fiber segment with compensation of linear phase shifts through application of a Faraday mirror. Originally proposed by Fermann *et al*. in [10], LSI lasers with all-PM configuration are fundamentally related to the well-known NPE mechanism [25] and were recently addressed in numerous studies as promising high-performance, all-PM alternatives to NALM/NOLM laser setups [26,27]. However, in contrast to widely applied non-PM NPE ring cavities, the polarization modes in the strongly birefringent PM fiber segment of the LSI cavity rapidly drift-off with ∼1 ps/m (PM980-XP fiber at 1030 nm), strongly suppressing the influence of cross-phase modulation in the accumulation of $\Delta\varphi_{nl}$. In contrast to NALM/NOLM lasers on the other hand, the configuration of the LSI prohibits a structural asymmetry with respect to the position of the gain fiber, hence the accumulation of a sufficient $\Delta\varphi_{nl}$ in the LSI relies entirely on the energy splitting ratio $\varepsilon = E_x/(E_x + E_y)$ between the fast (x) and slow (y) axis of the PM fiber, where the x axis is per definition parallel to the transmission axis of the PBS. The artificial SA is characterized by the transmission function $T(\Delta\varphi_{nl})$ that is highly tunable through the phase-bias rotation angles of HWP1 (θ_H) and QWP2 (θ_Q) as indicated in Fig. 1(b) for varying θ_H and θ_Q fixed at 0° and 45°. Here, $T(\Delta\varphi_{nl})$ is calculated with via application of the Jones formalism with an additional term to include the accumulated $\Delta\varphi_{nl}$, similar to [28]. The dependence of ε on the phase-bias rotation angles θ_H and θ_Q is visualized in Fig. 1(c). As the phase bias is coupled with the LSI asymmetry and the $T(\Delta\varphi_{nl})$ parameters, the settings of θ_H and θ_Q must ensure a large value of ε and a positive slope of $T(\Delta\varphi_{nl})$ for small signal values of $\Delta\varphi_{nl}$ (assuming a positive sign) in conjunction with a low non-saturable loss of the SA.

B. LSI-LMA Oscillator Characterization and Comparative Study

In the experiment, self-starting mode-locked operation of the LSI-LMA oscillator results from a state of the SA transmission function $T(\Delta\varphi_{nl})$ with $\theta_Q = 70°$ and θ_H adjusted in the range of 5° and 0°, with an energy splitting ratio ε of 0.75 and 0.66, respectively. With a net dispersion of $-0.121\ ps^2$, the laser self-starts into a multi-pulse soliton regime at about ∼6 W pump power. Reaching single-pulse operation requires a reduction of the pump power by 63% to ∼2.2 W. This well-known behavior (e.g., from NALM/NOLM oscillators) is associated with the insufficient accumulation of small-signal $\Delta\varphi_{nl}$ below a certain pump power threshold [28,29]. The continuous-wave lasing threshold is measured at 1.5 W pump power and the round-trip cavity loss excluding the non-saturable loss from the SA is estimated to be ∼65%. A measurement of the optical spectrum in the single-pulse regime at port T and port R with a center wavelength of ∼1058 nm for both cases is shown in Fig. 2(a). The maximum output pulse energy at port T is 5.4 nJ with an average power of 92 mW, obtainable by adjusting the output coupling ratio via rotation of QWP1. For the same working point, the pulse energy at port R reaches up to 4.3 nJ with 72 mW average power.

The initiation of mode-locked steady states in the dissipative or dispersion-managed soliton regime was observed at pump power levels between 7.5 and 8 W by the net dispersion through reduction of the grating distance. However, a stabilization for time periods longer than a few seconds was prohibited by occurring damage at the SMF tips or the MFAs within a few seconds, indicating the necessity of further high-power precautions such as anti-reflective coatings, fiber-endcaps, or passive/active cooling mechanisms.

To determine the influence of the LMA fiber configuration on characteristic laser parameters, the LSI-LMA oscillator is compared to a reference oscillator (RO) shown in Fig. 2(c). Instead of 25 µm core-diameter LMA fibers, the fiber segment of the RO is entirely based on standard PM fibers with a core diameter of 5.5 µm (Nufern, PM980-XP). The 976 nm pump light is supplied by a 1 W single-mode laser diode, coupled into the 0.5 m highly Yb-doped gain fiber (CorActive, Yb401-PM) through a wavelength-division multiplexer. The free-space arm is identical to the one used for the LSI-LMA oscillator and both repetition rate and the net dispersion are matched to 17.3 MHz and $-0.121\ ps^2$ via the passive fiber length, respectively. Together with a matched overall fiber length of ∼5.5 m, the high parameter similarity between both laser systems allows to assign occurring differences in mode-locked operation to the transition from a standard PM fiber to PLMA configuration. Self-starting mode-locked operation of the RO is obtained at a pump power of 0.75 W into a multi-pulse soliton regime. The phase-bias settings and the state of $T(\Delta\varphi_{nl})$ for this operation point are with $\theta_Q = 70° \pm 2°$ and θ_Q in the range of 5° and 0°, similar to the LSI-LMA oscillator. Entering a stable single-pulse working point requires subsequent reduction of the pump power by ∼70% to 0.14 W. The output pulse energies of the mode-locked RO in the single-pulse regime corresponding to the spectra shown in Fig. 2(b) are 0.15 nJ and 0.12 nJ for port T and port R, respectively. Hence, increasing the core size from 5.5 µm to 25 µm leads to an output energy scaling by a factor of 36. Compared to the RO, a distorted shape of the port R output spectrum can be observed for the LSI-LMA oscillator. A possible explanation could be distortions in the accumulated $\Delta\varphi_{nl}$ via multimode interactions and different gain dynamics, correlated with a resulting spectral reshaping by the NPE mechanism. In addition, both output spectra of the LSI-LMA oscillator show a 20 nm shift of the center wavelength from ∼1034 nm (RO) to ∼1058 nm. This can be explained with stronger re-absorption of the signal around 1030 nm, due to the increased doping concentration from $\sim 2.7*10^{20}\ cm^{-3}$ in the RO Yb-SMF to $\sim 1.4*10^{21}\ cm^{-3}$ in the Yb-PLMA fiber, required to compensate for the reduced overlap factor η_p of the multimode pump beam with the doped core.

The measured autocorrelation (AC) traces at port T and port R of the LSI-LMA oscillator are shown in Figs. 3(a) and 3(b) together with the Fourier transform limit (FTL), respectively. Assuming a $sech^2$ pulse shape with a deconvolution factor of 1.54, the pulse width (FWHM) at port T is 1.2 ps with a calculated FTL pulse duration of ∼0.6 ps. The shape and width of the FTL pulses are numerically retrieved from the output spectra in Fig. 2 via the fast Fourier transform algorithm. The output pulse at port T is negatively chirped due to the propagation of an average soliton according to the master equation [5,30], in conjunction with the structure of the oscillator shown in Fig. 1(a). The output pulse at port R in Fig. 3(b) is positively chirped with 1.3 ps duration compared to the calculated FTL of 0.36 ps. In the experiment, the RO output pulse energy has shown to be insufficient for clean AC measurements. From the output spectra, the FTL pulse durations at ports T and R are calculated to be 0.61 ps and 0.54 ps, respectively. Figure 3(c) shows the RF spectrum of the fundamental repetition frequency at ∼17.3 MHz with a signal-to-noise ratio (SNR) of 75 dB, indicating stable and low-noise mode-locked operation.

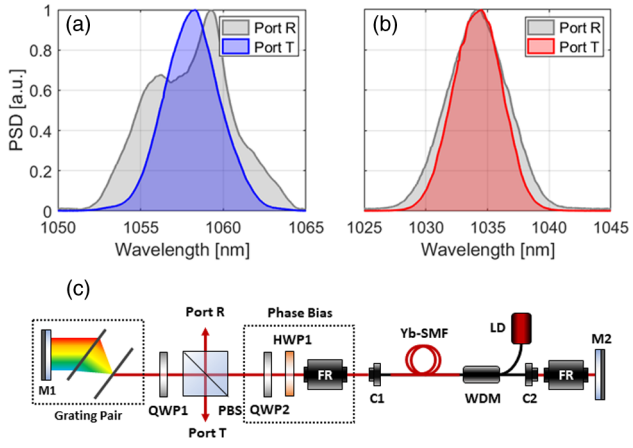

Fig. 2. (a) Measured spectra at port R (gray) and port T (blue) of the LSI-LMA oscillator in a soliton-like regime with a FWHM of 6 nm and ∼4 nm, respectively. (b) Measured spectra at port R (gray) and port T (red) of the reference oscillator with a FWHM of 6 nm and 5 nm, respectively. (c) Experimental setup of the reference oscillator. M, mirror; GP, grating pair; QWP, quarter-wave plate; HWP, half-wave plate; PBS, polarization beam splitter FR, Faraday rotator; C, collimator; Yb-SMF, ytterbium-doped single-mode fiber; LD, laser diode; WDM, wavelength-division multiplexer; FRM, Faraday rotator mirror.

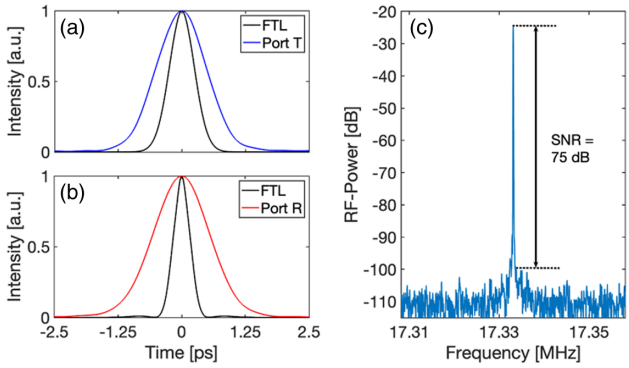

Fig. 3. (a) Measured output pulse (blue) and calculated Fourier transform-limited (FTL) pulse (black) at port T of the LSI-LMA oscillator with a FWHM of 1.2 ps and 0.6 ps, respectively. (b) Corresponding measured pulse (red) and calculated FTL pulse at port R with a FWHM of 1.3 ps and 0.36 ps, respectively. (c) RF spectrum of the LSI-LMA oscillator (port T) measured at the fundamental repetition rate of ∼17.33 MHz with a SNR of ∼75 dB.

C. Relative Intensity Noise

To further evaluate the stability and noise performance of the LSI-LMA oscillator, the frequency-resolved relative intensity noise (RIN) is investigated and compared between the two systems. To this end, the pulse train at the respective output port is detected with a fast and low-noise photodetector (Thorlabs DET08CFC) and the eighth harmonic of the received RF signal at 139.2 MHz is filtered with a tunable bandpass filter. Subsequently, the RF signal is amplified with a 10 dB low-noise trans-impedance amplifier (MiniCircuits ZX60-33LN-S+) to an RF power of −6.5 dBm, corresponding to a consistent shot noise level at −142.3 dBc. The amplitude modulation function of a signal-source analyzer (Keysight E552B) is then used to measure the single sideband frequency-resolved RIN spectral density. The results of the RIN measurements for the LSI-LMA and the RO at port T and port R are shown in Figs. 4(a) and 4(b), respectively.

In comparison with the RO, the magnitude of the RIN measured at port T shows a high similarity in the frequency range <50 Hz due to the identical environment of both laser systems in the laboratory. In the range from 50 Hz to ∼20 kHz, the noise of the LSI-LMA oscillator is significantly higher with a difference of up to 12 dB. A defining characteristic of the LMA oscillators RIN spectrum in this frequency range is a comb of resonant peaks at the utility frequency of 50 Hz and its higher harmonics. Hence, there is a strong indication that the increased RIN is not caused by intrinsic optical properties of the LSI-LMA laser nor the characteristics of the multimode laser diode, but instead by the influence of the power supply with insufficient electronic filtering/shielding. Therefore, the RIN integrated over the full measurement bandwidth reaches 0.063% for the LSI-LMA and 0.038% for the RO, as shown in Fig. 4(c). In the frequency range >20 kHz, associated with the fast optical dynamics in the cavity, the LSI-LMA port T output shows an improved RIN with decreased magnitude of the fluctuations by up to 5 dB and an int. RIN (20 kHz–5 MHz integration range) of 0.027% compared to 0.033% from the RO. An almost identical behavior can be observed in the RIN spectra and

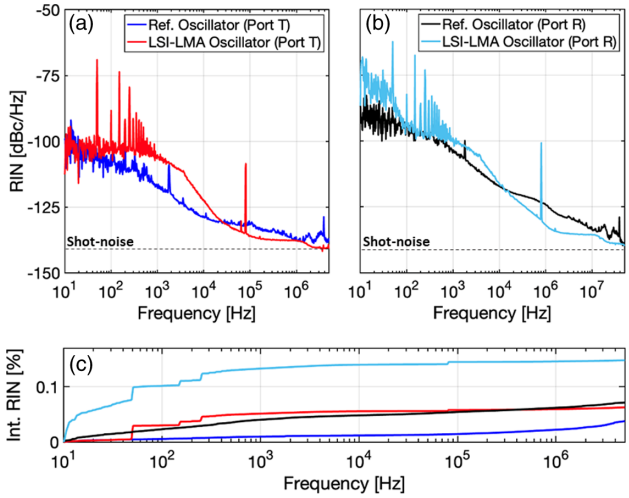

Fig. 4. (a) Frequency-resolved relative intensity noise (RIN) measured at port T of the reference oscillator (blue) and LSI-LMA oscillator (red). (b) RIN spectral densities measured at port R of the LSI-LMA (green) and reference oscillator (black). (c) Corresponding integrated RIN from 10 Hz to 5 MHz of 0.063% (LSI-LMA) and 0.038% (RO) at port T and 0.148% (LSI-LMA) and 0.071% (RO) at port R, respectively.

the integrated RIN at port R, as shown in Figs. 4(b) and 4(c), respectively. The RIN spectrum of the LSI-LMA output at port R has an increased magnitude between 50 Hz and 20 kHz compared to the RO, while it performs significantly better for frequencies >20 kHz with an improvement of up to 8 dB. With an integration over the complete measurement bandwidth, the integrated RIN at port R reaches 0.148% in the case of the LSI-LMA oscillator and 0.071% for the RO. In the frequency range >20 kHz, the int. RIN (20 kHz–5 MHz) of the LSI-LMA oscillator is lower with a value of 0.045% compared to 0.050% for the RO. A comparison of the fluctuations measured at port T and port R shows a noise difference for both laser systems. In both cases, the RIN spectral density measured at port T is significantly lower than at port R, leading to a difference in integrated values between the output ports of ∼3.7 dB in the case of the LSI-LMA oscillator and ∼2.7 dB for the RO. As we have shown in [31], this noise difference is characteristic for fiber oscillators mode-locked with non-linear fiber interferometers and can be explained with the dynamic response of the SA transmission $T(\Delta\varphi_{nl})$ to the intensity fluctuations of the intracavity pulse. Compared to the RO, the resulting RIN amplification of the reflected field at port R of the LSI-LMA oscillator combined with an increased noise coupling from the multimode pump diode further gives a possible explanation to the increased RIN spectral density in the low-frequency range <100 Hz.

3. CONCLUSION

In this work, we demonstrated an Yb-doped all-PM fiber oscillator mode-locked with an NPE-based self-stabilized interferometer that uses 25 µm core LMA fibers to avoid excessive non-linear phase shifts while scaling up the energy. Stable and self-starting mode-locked steady states in the soliton-like regime are demonstrated with a total pulse energy of ∼10 nJ and 170 mW average power distributed between two output ports.

An experimental comparison of the LSI-LMA oscillator with a reference oscillator constructed with 5.5 µm standard core-diameter fiber components shows that the 25 µm core LMA fibers allow an energy scaling by a factor of 36. Simultaneously, the RIN spectral density of the LMA oscillator shows a significant improvement for high offset frequencies >20 kHz by up to 8 dB. The results of this work demonstrate the possibility to implement LMA fibers in fiber oscillators mode-locked with LSIs for efficient energy scaling while preserving and even improving the stability and noise performance of the laser system. The successful demonstration of the LSI-LMA oscillator configuration is another important step in the ongoing search for high-power, environmentally stable, and ultra-low-noise fiber oscillators.

Funding. Deutsche Forschungsgemeinschaft (KA 908/18-1 PACE); European Research Council (609920).

Disclosures. The authors declare no conflicts of interest.

Data availability. Data underlying the results presented in this paper are not publicly available at this time but may be obtained from the authors upon reasonable request.

REFERENCES

1. K. Jung and J. Kim, "Subfemtosecond synchronization of microwave oscillators with mode-locked Er-fiber lasers," Opt. Lett. **37**, 2958–2960 (2012).
2. H. Chung, W. Liu, Q. Cao, L. Song, F. X. Kärtner, and G. Chang, "Megawatt peak power tunable femtosecond source based on self-phase modulation enabled spectral selection," Opt. Express **26**, 3684–3695 (2018).
3. M. Müller, C. Aleshire, A. Klenke, E. Haddad, F. Légaré, A. Tünnermann, and J. Limpert, "10.4 kW coherently combined ultrafast fiber laser," Opt. Lett. **45**, 3083–3086 (2020).
4. X. Xie, R. Bouchand, D. Nicolodi, M. Giunta, W. Hänsel, M. Lezius, A. Joshi, S. Datta, C. Alexandre, M. Lours, P.-A. Tremblin, G. Santarelli, R. Holzwarth, and Y. Le Coq, "Photonic microwave signals with zeptosecond-level absolute timing noise," Nat. Photonics **11**, 44–47 (2017).
5. H. A. Haus, "Mode-locking of lasers," IEEE J. Sel. Top. Quantum Electron. **6**, 1173–1185 (2000).
6. F. X. Kärtner, J. A. der Au, and U. Keller, "Mode-locking with slow and fast saturable absorbers-what's the difference?" IEEE J. Sel. Top. Quantum Electron. **4**, 159–168 (1998).
7. W. Hänsel, H. Hoogland, M. Giunta, S. Schmid, T. Steinmetz, R. Doubek, P. Mayer, S. Dobner, C. Cleff, M. Fischer, and R. Holzwarth, "All polarization-maintaining fiber laser architecture for robust femtosecond pulse generation," Appl. Phys. B **123**, 41 (2017).
8. N. Kuse, J. Jiang, C.-C. Lee, T. R. Schibli, and M. E. Fermann, "All polarization-maintaining Er fiber-based optical frequency combs with nonlinear amplifying loop mirror," Opt. Express **24**, 3095–3102 (2016).
9. J. W. Nicholson and M. Andrejco, "A polarization maintaining, dispersion managed, femtosecond figure-eight fiber laser," Opt. Express **14**, 8160–8167 (2006).
10. M. E. Fermann, L.-M. Yang, M. L. Stock, and M. J. Andrejco, "Environmentally stable Kerr-type mode-locked erbium fiber laser producing 360-fs pulses," Opt. Lett. **19**, 43–45 (1994).
11. M. Lezius, T. Wilken, C. Deutsch, *et al.*, "Space-borne frequency comb metrology," Optica **3**, 1381–1387 (2016).
12. Y. Ma, S. H. Salman, C. Mahnke, Y. Hua, S. Droste, J. Fellinger, A. S. Mayer, O. H. Heckl, C. M. Heyl, and I. Hartl, "Compact, All-PM fiber integrated and alignment-free ultrafast Yb:Fiber NALM laser with sub-femtosecond timing jitter," J. Lightwave Technol. **39**, 4431–4438 (2021).
13. U. Keller, K. J. Weingarten, F. X. Kärtner, D. Kopf, B. Braun, I. D. Jung, R. Fluck, C. Honninger, N. Matuschek, and J. Aus der Au, "Semiconductor saturable absorber mirrors (SESAM's) for femtosecond to nanosecond pulse generation in solid-state lasers," IEEE J. Sel. Top. Quantum Electron. **2**, 435–453 (1996).
14. R. S. Fodil, F. Amrani, C. Yang, A. Kellou, and P. Grelu, "Adjustable high-repetition-rate pulse trains in a passively-mode-locked fiber laser," Phys. Rev. A **94**, 013813 (2016).
15. J. Peng, L. Zhan, S. Luo, and Q. Shen, "Passive harmonic mode-locking of dissipative solitons in a normal-dispersion Er-doped fiber laser," J. Lightwave Technol. **31**, 2709–2714 (2013).
16. H. A. Haus and A. Mecozzi, "Noise of mode-locked lasers," IEEE J. Quantum Electron. **29**, 983–996 (1993).
17. R. Paschotta, "Noise of mode-locked lasers (part ii): timing jitter and other fluctuations," Appl. Phys. B **79**, 163–173 (2004).
18. P. Grelu and N. Akhmediev, "Dissipative solitons for mode-locked lasers," Nat. Photonics **6**, 84–92 (2012).
19. S. K. Turitsyn, B. G. Bale, and M. P. Fedoruk, "Dispersion-managed solitons in fibre systems and lasers," Phys. Rep. **521**, 135–203 (2012).
20. E. S. Lamb, L. G. Wright, and F. W. Wise, "Divided-pulse lasers," Opt. Lett. **39**, 2775–2777 (2014).
21. M. Edelmann, Y. Hua, G. Kulcsar, and F. X. Kärtner, "All-polarization-maintaining divided pulse fiber oscillator mode-locked with the optical Kerr effect," Opt. Lett. **46**, 6083–6086 (2021).
22. Z. Liu, Z. M. Ziegler, L. G. Wright, and F. W. Wise, "Megawatt peak power from a Mamyshev oscillator," Optica **4**, 649–654 (2017).
23. W. Liu, H. Shi, J. Cui, C. Xie, Y. Song, C. Wang, and M. Hu, "Single-polarization large-mode-area fiber laser mode-locked with a nonlinear amplifying loop mirror," Opt. Lett. **43**, 2848–2851 (2018).
24. M. Baumgartl, B. Ortaç, C. Lecaplain, A. Hideur, J. Limpert, and A. Tünnermann, "Sub-80 fs dissipative soliton large-mode-area fiber laser," Opt. Lett. **35**, 2311–2313 (2010).
25. M. Hofer, M. E. Fermann, F. Haberl, M. H. Ober, and A. J. Schmidt, "Mode locking with cross-phase and self-phase modulation," Opt. Lett. **16**, 502–504 (1991).
26. X. Liu, R. Zhou, D. Pan, Q. Li, and H. Y. Fu, "115-MHz Linear NPE fiber laser using all polarization-maintaining fibers," IEEE Photonics Technol. Lett. **33**, 81–84 (2021).
27. G. Liu, S. Ou, Q. Zhang, M. Zhang, X. Li, and Q. Bao, "All-polarization-maintaining linear fiber laser mode-locked by nonlinear polarization evolution with phase bias," Opt. Laser Technol. **142**, 107160 (2021).
28. A. S. Mayer, W. Grosinger, J. Fellinger, G. Winkler, L. W. Perner, S. Droste, S. H. Salman, C. Li, C. M. Heyl, I. Hartl, and O. H. Heckl, "Flexible all-PM NALM Yb:fiber laser design for frequency comb applications: operation regimes and their noise properties," Opt. Express **28**, 18946–18968 (2020).
29. C. Aguergaray, N. G. R. Broderick, M. Erkintalo, J. S. Y. Chen, and V. Kruglov, "Mode-locked femtosecond all-normal all-PM Yb-doped fiber laser using a nonlinear amplifying loop mirror," Opt. Express **20**, 10545–10551 (2012).
30. F. X. Kärtner, I. D. Jung, and U. Keller, "Soliton mode-locking with saturable absorbers," IEEE J. Sel. Top. Quantum Electron. **2**, 540–556 (1996).
31. M. Edelmann, Y. Hua, K. Şafak, and F. X. Kärtner, "Intrinsic amplitude-noise suppression in fiber lasers mode-locked with nonlinear amplifying loop mirrors," Opt. Lett. **46**, 1752–1755 (2021).